THERMAL EFFECTS IN HIGH POWER CW FIBER LASERS

Marc-André Lapointe*, Stephane Chatigny, Michel Piché, Michael Cain-Skaff, Jean-Noël Maran,
CorActive High-Tech, 2700 Jean-Perrin, suite 121, Québec, Canada, G2C 1S9

ABSTRACT

The thermal degradation of double clad optical fiber coatings is known to be the prime limiting factor for the operation of high power CW fiber lasers. In this paper, we conduct a study of thermal effects in high power CW fiber lasers. A particular focus is put on heating at the splice points and in the doped fiber due to the quantum defect in 100-W class CW fiber lasers. A theoretical model and experimental measurements taken with a high resolution IR camera on 125 to 400 μm diameter fibers are presented. Thermal contact resistance between the fiber and its heat sink are considered in the conduction heat transfer model and measured for different geometries. Proper designs for cooling apparatus are proposed and optimization of the active fiber is discussed. Some predictions for power scaling and temperature management of fiber lasers to kW power level are also described.

Keywords: high power CW fiber lasers, thermal effects, optical fiber splices, cooling designs, thermal measurements, acrylate degradation, thermal contact resistance.

1. INTRODUCTION

High power fiber lasers (HPFL) have generated a lot of attention over the past few years. Multi-kilowatt implementations of multimode HPFL and kilowatt implementation of singlemode (SM) HPFL have been achieved and commercial products are already available on the market [1]. The state-of-the-art demonstration of single mode operation of a fiber laser is currently at 6kW [2] and prediction of SM operation at power level exceeding 30kW has been made [3]. Their capability to maintain an excellent beam quality at high power is one of their main advantages. This interesting feature comes from the geometry of the gain medium, a very long and thin cylinder with a very large surface to volume ratio, allowing for an exceptional capacity of heat dissipation and hence a reduction of thermal lensing effects when compared to rod type solid state lasers. [4] have found no inherent limitations to power scaling of fibers. However, one should keep in mind that double clad optical fibers (DCOF) are surrounded by a polymer coating of limited tolerance to heat. Most of the time, the maximum heat load sustainable by these layers will set the maximum output power achievable by the fiber laser.

This paper intends to provide simple tools to evaluate the range of possible operation temperature for active fibers and fiber to fiber splices. Although the cross-flow convection is also presented, we will focus our attention on the conduction cooling scheme. Moreover, we will also consider the thermal contact resistance, a factor which is mostly neglected in the literature but reveals to be a very important parameter for the thermal management of active fibers and splices. If the thermal contact resistances are neglected, the conduction heat transfer model fails by overestimating the heat load capabilities of DCOF. This paper emphasizes the understanding of heat transfer in active fibers and its cooling apparatus, with the final objective of minimizing splice heating which is critical for the reliability of laser systems.

* marc-andre.lapointe@coractive.com; phone 1 418 845-2466 #236; fax 1 418 845-2609; www.coractive.com

2. ONE-DIMENSIONAL THERMAL MODEL OF A LONG CYLINDER

This section contains the derivations of the one-dimensional heat equation in cylindrical coordinates use d to obtain a thermal model of the optical fiber and its cooling apparatus. Presentation of cross-flow convective heat transfer model is also described. This section is necessary to understand how the active fiber is well represented by this model. This model will allow the calculation of the thermal contact resistance from experimental data.

2.1 Heat conduction

An optical fiber can be represented by a successive superposition of N long cylindrical layers. Each layer n is characterized by a radius R_n, an outer surface temperature T_{B_n}, an inner surface temperature T_{A_n}, a uniform rate of heat generation per unit volume $\dot{q}_n$, a heat transfer rate per unit length generated by previous layers q'_n and a constant thermal conductivity k_n. A schematic of the one-dimensional model is shown in Figure 1.

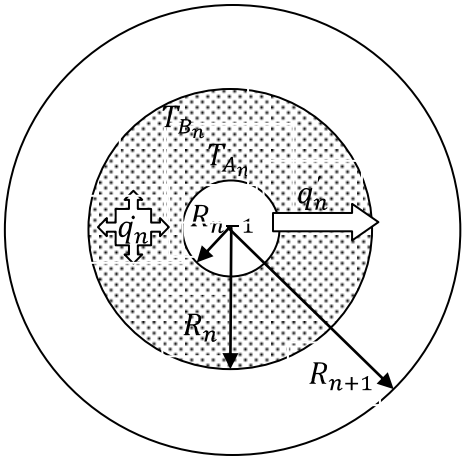

Figure 1. One-dimensional representation of N superposed cylindrical layers in consideration of heat generation.

The following heat equation [5] is used to obtain the temperature distribution in a long cylinder L at steady-state for a constant thermal conductivity k_n.

$$\frac{1}{r}\frac{d}{dr}\left(r\frac{dT}{dr}\right)+\frac{\dot{q}_n}{k_n}=0 \tag{1}$$

This equation is valid in the regime where the longitudinal heat transfer is negligible as compared to the radial heat transfer. This regime is valid when the length of the cylinder is much longer than its cross section ($L \gg R_N$). Eq. (1) is a second order partial differential equation and its resolution produces two constants whose values depend on boundary conditions. The solution of Eq. (1) is the sum of two contributions:

(a) the temperature contribution $T(r)_n - T_{B_n}$ from the internal heat generation source,

(b) the temperature contribution from the heat flow through the medium.

In order to obtain the contribution from (a), the thermal insulation boundary conditions need to be applied:

$$T(r)_n - T_{B_n} = \frac{\dot{q}_n}{4k_n}(R_n^2 - r^2) + \frac{\dot{q}_n}{2k_n}\left(R_{n-1}^2 \ln(r) - R_{n-1}^2 \ln\left(R_n\right)\right) \tag{2}$$

By applying the heat flux boundary conditions, the solution to (b) is:

$$T(r)_n - T_{B_n} = \frac{q'_n}{2\pi k_n}\ln\left(\frac{R_n}{r}\right) \tag{3}$$

Heat diffusion is often compared to electrical charge diffusion. A temperature difference appears when heat flows through a thermal resistance R'_n (m·K/W). From Eq. (3), it is easy to see this analogy. By evaluating Eq. (3) at $= R_{n-1}$, one finds:

$$T_{A_n} - T_{B_n} = \frac{q'_n}{2\pi k_n} \ln\left(\frac{R_n}{R_{n-1}}\right) = q'_n \cdot R'_n \tag{4}$$

This form is also obtained in convective heat transfer mode and is especially suitable for thermal contact resistances. There is a thermal contact resistance between two layers when interface imperfections are present. A thermal contact resistance R''_{tc} is a constant, generally of units m^2·K/W, that is used to represent a thin layer of complex heat transfer as shown in Figure 2.

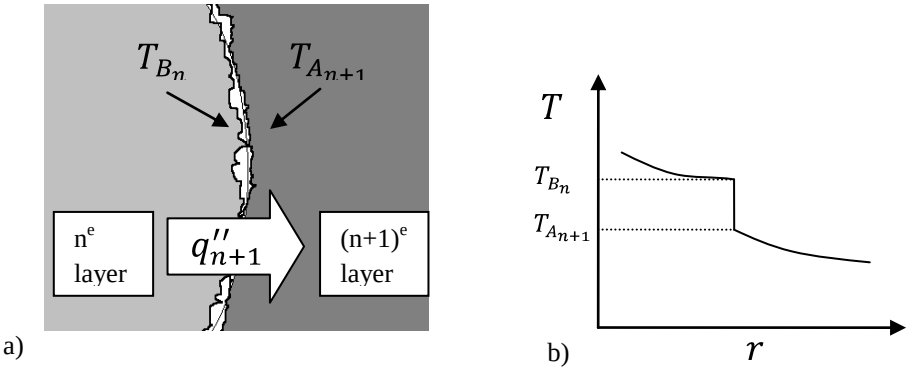

Figure 2. a) Interface presenting a complex heat transfer function that could be represented by a thermal contact resistance. b) The associated temperature drop at this interface.

These contact resistances might be present at interfaces between glass layers in the optical fiber, at the interface between glass and coating layers, at the interface between different coating layers and between the fiber and its heat sink. However, since the production process of optical fibers controls accurately the quality of the glass interfaces and the application of the coating layers, the main contributor to the overall thermal contact resistance is clearly the interface between the fiber and the heat sink. At this interface, there is a possibility that R''_{tc} is large enough to create an important temperature drop even if a filling material is present. In such a case, the internal layers will be warmer than expected.

Each pair of layers is linked together by a thermal contact resistance per unit surface R''_{tc} and a heat flux q'':

$$T_{B_n} = R''_{tc} q''_{n+1} + T_{A_{n+1}} \tag{5}$$

For cylindrical geometries, the heat flux is defined by:

$$q''_n \equiv \frac{q'_n}{2\pi R_n} \tag{6}$$

Because the heat flux gives a temperature gradient, a known temperature is necessary to evaluate the absolute temperature of the system. This is not a problem since the temperature for $r \to \infty$ can be fixed to the ambient temperature. For computation with optical fibers, if the last layer, generally a heat sink of considerable thickness, has a thermal conductivity significantly higher than that of the previous layer, a good approximation of absolute temperature is obtained by fixing T_{B_N} to be the ambient temperature.

2.2 Cross-flow convection

Heat transfer by external flow is the only other significant heat transfer mode for an optical fiber. Radiation heat transfer has been studied in other works [6,7] but the limitation of fiber temperature set by the coating limits the impact of

radiation to a negligible value. It can also be shown [7], that free convection is an order of magnitude less efficient than conduction for dissipating heat from an optical fiber. Figure 3 shows a schematic of a cylinder of radius R_i, in a cross-flow of a fluid at a speed V and a temperature T_∞, that produces a heat transfer per unit length q'.

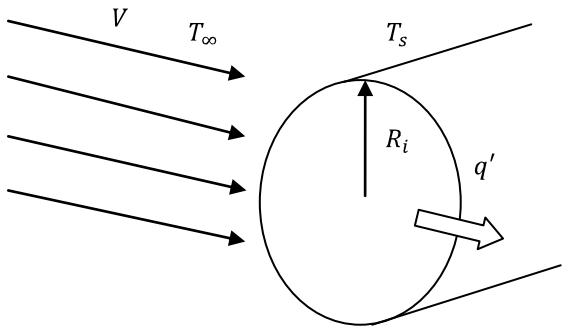

Figure 3. One-dimensional representation of cross-flow heat transfer with a long cylinder

The surface temperature T_s is obtained from Newton's law of cooling [5]:

$$\overline{h'} = \frac{q'}{2\pi R_i (T_s - T_\infty)} \tag{7}$$

The average convection heat transfer coefficient per unit length $\overline{h'}$ is related to the Nusselt number $\overline{NU}_D$:

$$\overline{h'} = \overline{NU}_D \frac{k}{2R_i} \tag{8}$$

The Churchill relation, which gives the Nusselt number, covers the entire range of Reynolds number Re_d for all values of $Re_d Pr > 0.2$, where Pr is the Prandtl Number constant of the fluid;

$$\overline{NU}_D = 0.3 + \frac{0.62 Re_D^{1/2} Pr^{1/3}}{\left[1+(0.4/Pr)^{2/3}\right]^{1/4}} \left[1 + \left(\frac{Re_D}{282\,000}\right)^{5/8}\right]^{4/5} \tag{9}$$

The Reynolds number Re_d is an important quantity that determines the boundary layer transitions of the flow and is defined as $Re_d \equiv \frac{2VR_i}{v}$ where v is the kinematic velocity of the fluid. All fluid properties are taken at the film temperature $T_f \equiv \frac{T_s + T_\infty}{2}$.

3. APPLICATION TO DOUBLE-CLAD ACTIVE FIBERS

3.1 Temperature distribution of double-clad active fibers

The active fiber, schematized in Figure 4, is considered to produce uniform heat generation in its core $\dot{q_0}$, whose units are W/m^3. This heat generation comes mainly from the quantum defect of the system. $\dot{q_0}$ is considered known as it is obtained from the pump absorption α (dB/m), the pump power P through a section of interest of length dL, the signal and pump wavelengths, λ_s and λ_p respectively, and the radius of the core R_0. Because there is heat generation only in the core, each other layer has the same heat transfer i.e $q_1' = q_2' = q'$. The heat generation $\dot{q_0}$, the heat load q' and the pump absorption α are related to each other:

$$\dot{q_0} = \left(1 - 10^{-\alpha * dL/10}\right) \frac{P\left(1 - \frac{\lambda_p}{\lambda_s}\right)}{\pi R_0^2} = \frac{q'\, dL}{\pi R_0^2} \tag{10}$$

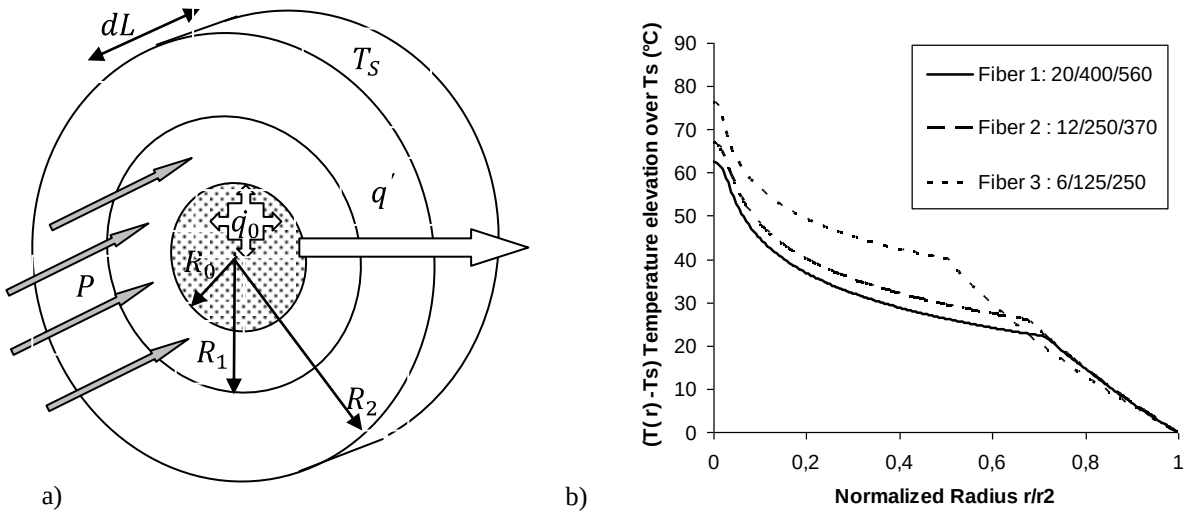

Figure 4. a) One-dimensional representation of an active fiber with uniform heat generation in its core. b) Temperature profile in radial direction for a heat transfer rate of 100 W/m for 3 fiber sizes.

In Figure 4 b), the parameters are $k_0 = k_1 = 1.38\,\mathrm{W/(m{\cdot}K)}$, $k_2 = 0.24\,\mathrm{W/(m{\cdot}K)}$ and layers radius are in the form $R_0/R_1/R_2$. Simple calculations provide the temperature profile for these geometries for any other heat transfer rate; $T(r)_b = T(r)_a q'_b/q'_a$. A 100 W/m heat load is equivalent to 2.9 kW of pump power at 915nm in an ytterbium doped fiber with 1 dB/m of pump absorption. At identical heat loads, Figure 4 b) shows that the temperature gradient in the coating is higher for a smaller cladding size when a similar thickness of acrylate coating is applied to the fiber. In practice, the acrylate coating thickness is generally 50 to 80 μm whatever the cladding size. As it can be noticed in Figure 4 b), the thermal gradient in the coating is around 30 – 40 degrees for a heat load of 100 W/m. In 100-W class lasers, because the heat load is only 5 to 15 W/m, thermal gradient in the coating can be considered almost uniform as it represents only 2 to 5 degrees over the surface temperature.

3.2 Optimization of the active fiber

It was previously suggested in [8], that there is an optimal thickness of acrylate coating that increases cooling of the active fiber in forced convection. Fiber optimization is possible for both the convective mode and the conductive mode, as long as one consider a thermal contact resistance $\mathrm{R}''_{\mathrm{tc}}$ between the fiber and the cooling apparatus.

The maximum temperature of the coating decrease proportionally with the total thermal resistance R'_{tot} of the system. R'_{tot} is the sum of the thermal resistance due to the coating R'_{cond} and the thermal resistance of the convective fluid R'_{conv}. The optimal radius for convective heat transfer mode is given as:

$$R_2 = \frac{k_2}{h} \tag{11}$$

As Re_d depends upon the external radius and the air cross-flow velocity V, the convective heat coefficient must be calculated for each radius R_2 and fluid velocity V to obtain the optimal radius. The fluid properties of air change significantly over the range from 25° to 100°C which creates a temperature dependence of the convective heat transfer coefficient. For the conductive mode, if materials properties are not temperature dependent, optimal radius is obtained more directly. First, the total resistance of the system is expressed as:

$$\mathrm{R}'_{\mathrm{tot}} = \frac{1}{2\pi k_2}\ln\left(\frac{R_2}{R_1}\right) + \frac{\mathrm{R}''_{\mathrm{tc}}}{2\pi R_2} \tag{12}$$

The optimal radius R_2 is obtained by solving Eq. (12) for $\frac{d\mathrm{R}'_{\mathrm{tot}}}{R_2} = 0$, which leads to:

$$R_2 = k_2 \cdot \mathrm{R}''_{\mathrm{tc}} \tag{13}$$

However, the optimal thickness for both heat transfer modes is greatly dependent on the quality of cooling as presented in Figure 5. Thus, looking for an optimal thickness of coating for convection is irrelevant as the air speed is hardly known and efficient uniform air flow is difficult to get. Actual fibers with 50 µm to 80 µm of coating thickness should be cooled with high speed air flow of over 10m/s to maximize the cooling efficiency. For comparison, a 20/400/560 active fiber cooled in a respectable 15m/s air flow is limited to a heat load of 50W/m at 80°C. This heat load is equivalent to 1.4 kW of pump power at 915nm in an ytterbium doped fiber with 1 dB/m of pump absorption. In the case of cooling by conduction, optimal coating thickness is dependent on the thermal contact resistance between the fiber and the heat sink. On the other side, for a typical good thermal contact resistance $\mathrm{R}''_{\mathrm{tc}}$ varying from 5 to 10 $\mathrm{m}^2 \cdot \mathrm{K/W}$, the actual coating thickness is appropriate.

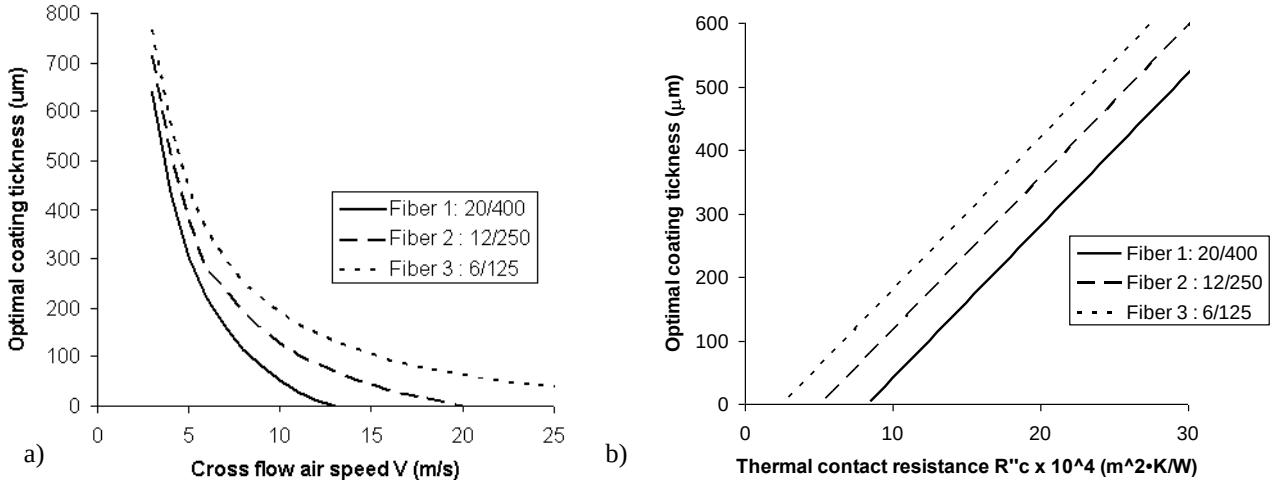

Figure 5. Optimal coating thickness as function of a) the cross flow air speed in a convective heat transfer mode, b) the thermal contact resistance in a conductive cooling scheme. Air properties were taken at a film temperature of 36°C.

4. EXPERIMENTAL RESULTS

4.1 Evaluation of coating emissivity

Because temperature measurements with an IR thermal camera are greatly sensitive to the emissivity of the measured object, it is important to know the emissivity of the acrylate coating. A fast evaluation of coating emissivity was done by heating a fiber bundle in a temperature controlled chamber and by measuring its temperature with a thermal camera immediately after being removed from the chamber. The measurement must be made in a room at ambient temperature since the emissivity is less than 1. Otherwise, the coating will reflect the radiation of the chamber and the measurement of the emissivity will be less accurate. For a bundle of fiber at 75°C, the measurement with a thermal camera, with a configured emissivity of 1, provided an average of 71.0°C ± 0.5. The 4°C difference in the temperature, between the real and the measured values, corresponds to a coating emissivity of 0,91± 0,02.

4.2 Evaluation of thermal contact resistance

To evaluate the values of thermal contact resistances $\mathrm{R}''_{\mathrm{tc}}$ for each geometry and interstitial material, all other parameters must be known. The experiments consist of using precisely machined grooves with an active fiber of known parameters to measure the surface temperature T_s and obtain the average thermal contact resistance $\mathrm{R}''_{\mathrm{tc}}$. Figure 6 shows the geometry of the grooves used for the experiment. This heat sink is maintained at a constant temperature T_∞ during the experiment.

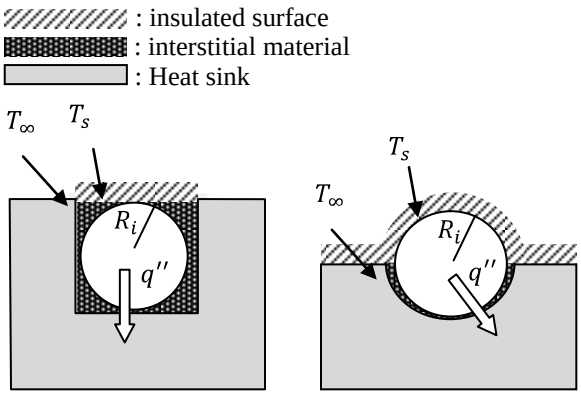

Figure 6. Schematic representation of the experimental setup for determination of thermal contact resistance.

Although the geometries of Figure 6 are not fully cylindrical, results from cylindrical conduction model can still be used. Some assumptions are to be considered to obtain an approximation of R''_{tc} with Eq. (5). The first is that heat transfer from fiber to air is small enough to consider air as a thermal insulator. The second is that the measured surface temperature exposed to air is close to the actual temperature of the fiber which is uniform in the radial direction. Third, the thermal contact resistance is invariant with temperature. Finally, the temperature of the heat sink T_∞ is considered uniform and, without any heat load, T_s should be equal to T_∞. With all these assumptions, the heat load q' is obtained from Eq. (10) and must be divided by the perimeter, which is the junction between the heat sink and the fiber, to get the heat flux q''. Because the grooves do not perfectly match the fibers, the interstitial fluid has a significant thickness. Thus, the chosen perimeter will affect the value of R''_{tc}. For convenience, the perimeter is calculated from the groove geometry. The aluminum heat sink used in the experiment presents three half-pipe grooves and three square grooves to accommodate three different sizes of active fibers. In some measurements an optical epoxy is used as interstitial material. Its thermal conductivity is similar to the coating conductivity. Temperature measurements were done with and without an interstitial fluid. It is important to note that the ytterbium doped fibers were simply dropped in the grooves without any external pressure. The results of the experiments and numerical calculations are shown in Table 1.

Table 1. Thermal contact resistance for three fibers sizes and two heat sink geometries.

Parameters	Fiber 1:20/400/560		Fiber 2:12/250/370		Fiber 3:6/125/250	
Geometry	600µm	300µm	400µm	200µm	300µm	150µm
Fiber external radius (µm)	565		371		255	
Perimeter of the geometry (µm)	1800	942	1200	628	900	471
Pump absorption at 915nm α at test position(dB/m)	0,55		0.65		0,4	
Quantum defect $\frac{\lambda_p}{\lambda_s}$	0,89		0.94		0,89	
Pump power at test position (W)	250		102		100	
Heat load at test power (W/m)	3.50		0.92		1.02	
Temperature elevation of the fiber **with** an interstitial material (°C)	8.4	9.1	1.3	3.1	1.0	3.2
Temperature elevation of the fiber **without** an interstitial material (°C)	18.2	30.5	4.6	6.8	4.1	3.5
R''_{tc} x10^{-4} **with** an interstitial material (m^2·K/W)	40	21	16	19	8	14
R''_{tc} x10^{-4} **without** an interstitial material (m^2·K/W)	88	69	53	41	34	15

Many assumptions and parameters calculations are made to obtain an approximation of the thermal contact resistance. Thus, uncertainty on the values of R''_{tc} is particularly high. R''_{tc} can be, in reality, two times larger or smaller than the determined value. Although the given R''_{tc} is roughly determined, its order of magnitude shows that thermal contact resistances are a major contributor to the heating of optical fibers. R''_{tc} will vary greatly depending on the designs and quality of the methodologies. Thus, the results from Table 1 cannot determine accurately the temperature of the fiber for another cooling apparatus, whose value of R''_{tc} will differ. There are many ways to minimize R''_{tc}: thermal contact resistances are, in general, highly pressure dependent and very sensitive to surface roughness. For example it is worthless to seek for a highly conductive heat sink material when machining surface roughness can be improved. Figure 7 shows that an improvement in surface roughness of the heat sink used in this experiment is still possible.

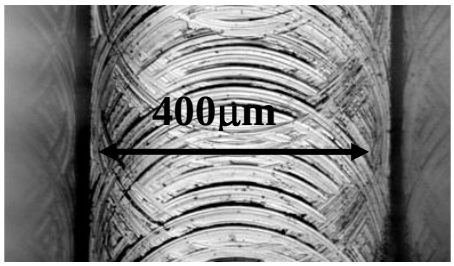

Figure 7. Microscope images of the 400µmX400µm groove.

By knowing a possible range of values of R''_{tc}, approximation of active fiber temperature as a function of pump power is easily achieved from Eq. (12) and from Eq. (4). Thus, from the results of Table 1, the range of maximal pump power for an internal coating temperature of 80°C for the three fibers sizes is considerably high. Keeping an active fiber within a safe temperature range with a 40 to 100 W/m of heat load should not be too challenging. Higher heat load is possible with careful design. Although the heat load capabilities of 125 µm DCOF is high, it is doubtful that a 125 µm fiber can be pumped with 3 kW of pump power from a single point of injection because quantum defect is not the only heat generation process involved in an all-fiber design. The important result from Table 1 and Eq. (12) is that thermal management of active fibers, with absorption of 0.5 to 1 dB/m at 915 nm, is not a limiting factor for HPFL. However, as we will see in section 5, this heat load from the quantum defect must be added to the contribution of the pump guide splice loss.

4.3 Evaluation of critical coating temperature

Because high resolution thermal cameras are expensive equipments and their bolometer sensors can be damaged if exposed to high temperature in their field of view, we will avoid exposing our instrument to a burning fiber. However, as seen in section 2, the temperature rise of an optical fiber is linear with the internal heat load. Thus, by measuring the coating temperature rise versus injected pump power at low power, it is still possible to extrapolate the temperature directly from the injected pump power at the critical surface temperature when the fiber coating will ignite. The easiest test to obtain an approximation of the critical temperature of the coating is to splice a DCOF to a single clad fiber (SCOF). The SCOF will rapidly absorb the pump power and will provide a considerable heating without much power. By using the worst cooling possible of the splice, the heat load is minimized for a given temperature. In this case, maximum internal coating temperature can be considered to be equal to the surface temperature. This simple experiment shows that the coating of SCOF will catch fire at approximately 170±10°C. On the other hand, splices have exhibited a great variability of the critical temperature. Some splices will ignite at 130°C while some resist at an extreme 210°C. The critical coating temperature of splices depends on the depth of the heat generation and the origin of heating. Contamination between the glass cladding and the coating can explain a low tolerance to temperature of certain recoated splices. For short-term operation, keeping the coating temperature below 120°C, with consideration of internal temperature distribution, should prevent the destruction of the fiber. However polymers are complex materials, their thermal and optical properties can change over time and degradation can occur due to high temperature or humidity. Coating temperature at 80°C is often considered a safe long-term temperature.

5. DISCUSSION ON THERMAL MANAGEMENT OF SPLICES

Thermal management of splices in high power fiber lasers is challenging because important pump loss absorption adds to the heat load of the active fiber. In a recoated splice, as sketched in Figure 8, heating is due to absorption in the coating material of a fraction of the pump power scattered by distortions of the waveguide. Most of the time the signal splice losses will not contribute to heating because it is mostly trapped in the pump guide of the DCOF. Coating of DCOF is almost 100% transparent and normally will not absorb light on a short length. In such a situation the heat load is spatially distributed and does not represent much of a problem. However, any surface or interface imperfection might generate micro-cavities that will significantly increase the photon path length and will increase tremendously the probability of absorption in a relatively small volume. In Figure 8 a part of the pump light coming from the left is scattered through the splice due an improper splicing parameters or cladding geometry mismatch. This power hits the right stripping point where some power is absorbed by interface irregularities. The deformation at the splice point might also be responsible for the heating directly at the splice point. It should be noted that the thermal heating of the splice is greatly dependent upon the geometrical extent of the incoming pump signal. With the current tapered fiber bundle pump combining technology, 125-µm splices are thermally more challenging than other fiber sizes because the filling factor of commercial 7→1 125 µm pump combiners is at the maximal capacity of 125-µm DCOF. Thus, a substantial amount of pump power is barely guided by the fiber cladding. Light rays with high NA, with respect to the waveguide, are more sensitive to distortions and will be lost at the splice point. On the other hand, splices with larger cladding fibers do not have those high pump losses because the pump branch count in 250-µm and 400-µm combiners is still far from the maximum gathering capability of low index coated DCOF.

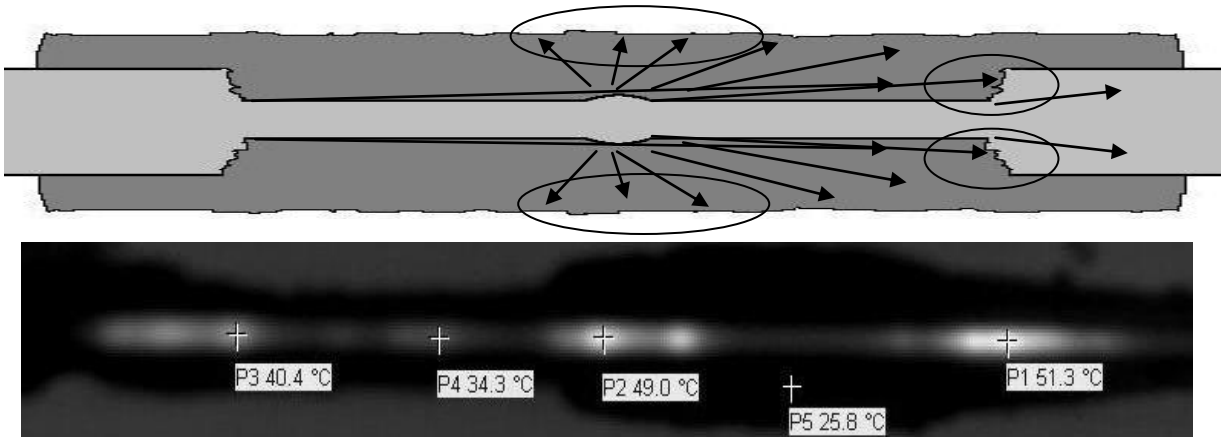

Figure 8. Top: representation of pump scattering (arrows) and heating spot (surrounded regions) of a left pumped recoated splice. The image at the bottom is a thermal measurement of a 330-W left pumped recoats on a 400-µm fiber to fiber splice, cooled in an aluminum slot groove of 800-µm. The two major hot spots are due to the cladding deformation at the splice point and to the irregular interface at the stripping point.

Because surface quality influences thermal contact resistances and light absorption in the coating, better recoat methodologies must be applied. Figure 9 shows a recoat from a telecom reacoater that produces a frosted like look of the recoat surface.

Figure 9. Left image is a 10X microscope view of the surface of a 800-μm recoat on a 400-μm fiber. Recoats from standard telecom reacoater have a frosted look surface. Right image is a typical stripping point.

However, with a careful approach and optimized recoat methodologies, a lower thermal contact resistance and lower pump losses can be achievable as shown in Figure 10. In this example the splice has a surface temperature rise of only 0,014 K/W. Thus, it could be pumped with over 4kW of pump power within acceptable long term temperature limit.

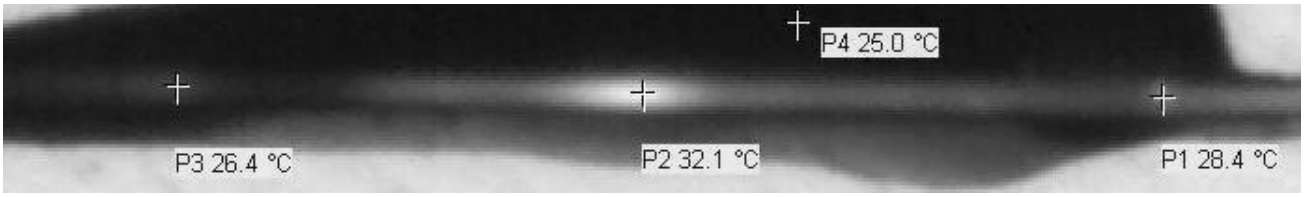

Figure 10. Thermal image of a 520-W left pumped recoats of a 400-μm round fiber spliced to a 400-μm octagonal doped fiber. The splice is cooled in an aluminum slot groove of 600-μm. 19 laser diodes of 0.22NA, with a 19 to 1 pump combiner, are used to pump this splice.

6. CONCLUSION

An analytical approach with consideration of thermal contact resistances is proposed to evaluate the heat load capabilities of optical fibers and splices of HPFL. Optimal coating thickness analysis demonstrates that, for existing optical fibers, coating thickness is appropriate for high cooling capabilities. The values of thermal contact resistance for different fiber sizes are obtained. Active fibers are demonstrated to be capable, with a minimal effort of cooling design, of considerable heat loads of approximately 40 to 100W/m, which is less than predictions without the consideration of thermal contact resistance. The thermal management of splices is more challenging than that of active fibers but, in this paper, a splice of 0,014 K/W of temperature rise capable of sustaining 4kW of pump power is reported.

ACKNOWLEDGEMENTS

This work has benefited from the financial support from CorActive High Tech and Laval University. Marc-André Lapointe was supported by a FQRNT-NSERC scholarship awarded through the BMP “Photonics” program managed in collaboration with the Canadian Institute for Photonic Innovations (CIPI).

REFERENCES

[1] IPG Photonics, http://www.ipgphotonics.com.

[2] Gapontsev, D., "6kW CW Single mode Ytterbium fiber laser in all-fiber format", 21st Annual Solid State and Diode Laser Technology review, 258 (2008).

[3] Dawson, J.W. , Messerly, M.J. , Beach, R.J., Shverdin, M.Y. , Stappaerts, E.A. , Sridharan, A.K., Pax, P.H., Heebner, J.E. , Siders, C.W. , Barty, C.P.J. , "`Analysis of the scalability of diffraction-limited fiber lasers and amplifiers to high average power", Opt. Exp., vol. 16 no. 17, 13240-13266 (2008).

[4] Brown, D.C, Hoffman, H.J., "Thermal, Stress, and Thermo-Optic Effects in High Average Power Double-Clad Silica Fiber Lasers", IEEE J. of Quant. Electronics, 37, 2 (2001).

[5] Incropera, F., DeWitt, D., [Fundamentals of Heat and Mass Transfer], John Wiley & Sons, Hoboken (2002).

[6] Li, J., Duan, K., Wang, Y., Cao, X., Zhao, W., Guo, Y., Lin, X., "Theoretical analysis of the heat dissipation mechanism in Yb3+-doped double-clad fiber lasers", Journal of Modern Optics, Vol. 55 No. 3, 459–471 (2008).

[7] Yan, P., Xu, A., Gong, M., "Numerical analysis of temperature distributions in Yb-doped double-clad fiber lasers with consideration of radiative heat transfer", Optical Engineering, 45(12), 124201 (2006).

[8] Zintzen, B., Langer, T., Geiger, J., Hoffmann, D., Loosen, P., "Optimization of heat transfer in multi-kW-fiber-Laser", Proc. SPIE 6873, 687319-1 (2008).